Journal of Magnetic Resonance 214 (2012) 237–243

Contents lists available at SciVerse ScienceDirect

Journal of Magnetic Resonance

journal homepage: www.elsevier.com/locate/jmr

A tunable general purpose Q-band resonator for CW and pulse EPR/ENDOR experiments with large sample access and optical excitation

Edward Reijerse [a,*], Friedhelm Lendzian [b], Roger Isaacson [c], Wolfgang Lubitz [a,*]

[a] Max-Planck-Institut für Bioanorganische Chemie, 45470 Mülheim an der Ruhr, Stiftstr. 34-36, Germany
[b] Max-Volmer-Laboratorium, Institut für Chemie, Technische Universität Berlin, Straße des 17. Juni 135, 10623 Berlin, Germany
[c] Department of Physics, University of California, San Diego, 9500 Gilman Dr., La Jolla, CA 92093, USA

ARTICLE INFO

Article history:
Received 29 July 2011
Revised 11 November 2011
Available online 30 November 2011

Keywords:
Microwave resonator
Q-band
Pulse EPR
ENDOR
ELDOR

ABSTRACT

We describe a frequency tunable Q-band cavity (34 GHz) designed for CW and pulse Electron Paramagnetic Resonance (EPR) as well as Electron Nuclear Double Resonance (ENDOR) and Electron Electron Double Resonance (ELDOR) experiments. The TE_{011} cylindrical resonator is machined either from brass or from graphite (which is subsequently gold plated), to improve the penetration of the 100 kHz field modulation signal. The (self-supporting) ENDOR coil consists of four 0.8 mm silver posts at 2.67 mm distance from the cavity center axis, penetrating through the plunger heads. It is very robust and immune to mechanical vibrations. The coil is electrically shielded to enable CW ENDOR experiments with high RF power (500 W). The top plunger of the cavity is movable and allows a frequency tuning of ±2 GHz. In our setup the standard operation frequency is 34.0 GHz. The microwaves are coupled into the resonator through an iris in the cylinder wall and matching is accomplished by a sliding short in the coupling waveguide. Optical excitation of the sample is enabled through slits in the cavity wall (transmission ~60%). The resonator accepts 3 mm o.d. sample tubes. This leads to a favorable sensitivity especially for pulse EPR experiments of low concentration biological samples. The probehead dimensions are compatible with that of Bruker flexline Q-band resonators and it fits perfectly into an Oxford CF935 Helium flow cryostat (4–300 K). It is demonstrated that, due to the relatively large active sample volume (20–30 μl), the described resonator has superior concentration sensitivity as compared to commercial pulse Q-band resonators. The quality factor (Q_L) of the resonator can be varied between 2600 (critical coupling) and 1300 (over-coupling). The shortest achieved $\pi/2$-pulse durations are 20 ns using a 3 W microwave amplifier. ENDOR (RF) π-pulses of 20 μs (^{1}H @ 51 MHz) were obtained for a 300 W amplifier and 7 μs using a 2500 W amplifier. Selected applications of the resonator are presented.

1. Introduction

Electron paramagnetic resonance (EPR) spectroscopy is an important analytical tool in a variety of different research fields from chemistry, physics, and materials science to biological and medical research. An essential part of the EPR spectrometer is the microwave resonator, which accommodates the sample to be investigated and which determines the critical experimental parameters such as the sensitivity and time resolution.

For the most common EPR frequency band (X-band, ca. 9.5 GHz) a large variety of dedicated commercial microwave resonators are available [1], which have been optimized for different purposes like maximum sensitivity, small sample size, or highest time resolution (largest bandwidth).

Resonators which are designed to operate at X-band (9 GHz) frequencies are usually of a type which does not allow frequency tuning. For CW EPR the rectangular TE_{102} cavity serves as standard since it combines a reasonable filling factor with a relatively high quality factor (Q). In addition, it is not very susceptible to samples with dielectric losses. Also it can be easily combined with a cold finger cryostat which greatly simplifies sample loading. For specific applications like pulse EPR and (pulse) Electron Nuclear Double Resonance (ENDOR) the convenient TE_{102} cavity design usually has be abandoned due to the additional requirements of large bandwidth and the need to accommodate an RF coil. For these applications dedicated resonators have been developed [2–9]. Since X-band sources (Gunn oscillators and Klystrons) are usually tunable over a relatively wide range the need for cavity tunability is not very high.

For many applications, in particular for biological systems, a multi-frequency approach is required in order to unravel complex spectra. This includes EPR experiments at Q-band (35 GHz), W-band (94 GHz) and even higher frequencies (120, 240 up to

* Corresponding authors.
E-mail addresses: reijerse@mpi-muelheim.mpg.de (E. Reijerse), wolfgang.lubitz@mpi-mail.mpg.de (W. Lubitz).

1090-7807/$ - see front matter © 2011 Elsevier Inc. All rights reserved.
doi:10.1016/j.jmr.2011.11.011

275 GHz). At Q-band frequencies (35 GHz) the cylindrical TE_{011} cavity is the most frequently used resonator for multiple applications including pulse EPR and ENDOR [1]. This is because the relatively large size of the cavity body makes it easier to machine than scaled down versions of e.g. a TE_{102} cavity. Also it is quite straight forward to vary the resonance frequency by moving one or both plungers in and out. This is an important feature since at 35 GHz the usual microwave sources (Gunn oscillators) are not tunable over a wide range while in contrast the frequency shifts of the resonator upon inserting the sample can be appreciable. To combine a tunable TE_{011} cylindrical resonator with field modulation, rf coils (ENDOR) and optical excitation capabilities is quite challenging. Only a few groups have reported attempts in this direction. Already in the 70ties the group of Feher and Isaacson used a Q-band ENDOR resonator optimized for CW-ENDOR [Isaacson and Feher, private communication]. Also the Hoffman group [10] have successfully utilized a CW/pulse ENDOR Q-band resonator. Sienkiewicz et al. [11] described the first tunable Q-band ENDOR resonator. The groups of Schweiger and Jeschke have developed several specialized Q-band resonators e.g. for CW and pulse EPR [12], large microwave excitation pulse EPR and CW EPR [13] as well as large sample access pulse EPR and ENDOR [14]. Recently, also a tunable Q-band resonator was described optimized for ESE-ENDOR [15].

Our group specializes in pulse EPR and ENDOR at X- and Q-band on metalloproteins and radical proteins including photo excited systems [16–20]. Especially for Q-band pulse ENDOR measurements a cavity with a good filling factor and high ENDOR efficiency is required. The original Bruker ER 5106 QT low temperature Q-band resonator with ENDOR option did not fulfill these requirements as it was originally designed for CW EPR/ENDOR. Its successor, the dielectric model EN5107 is very efficient in microwave and RF power conversion but, at the same time, has a limited sample access (1.6 mm diameter). Since we required a CW/pulse ENDOR resonator compatible in sample access to the standard CW Q-band resonator (3 mm) we decided to develop and built a general purpose Q-band CW/pulse EPR/ENDOR resonator allowing optical access and large sample sizes. As will be shown, our improved resonator has several features which are particularly useful for pulse EPR/ENDOR on metalloproteins and (bio)radicals. The internal 2 turn ENDOR coil is extremely robust and can be used in CW ENDOR up to 500 W and in Pulse ENDOR up to 2.5 kW rf power. In addition, the resonator has good CW EPR properties (1 mT modulation at 100 kHz) and a generous light access (3 mm spot, ~60% transmission). The 3 mm sample tube access affords high sensitivity for biological samples at low concentrations. The same sample tubes can be used with high sensitivity also for 9.5 GHz standard frequency EPR spectrometers. This allows measuring one and the same sample tube at 9.5 GHz and at 34 GHz EPR, which is often an important requirement for investigating biological systems.[1]

2. Technical description

The cavity body used in pulse EPR/ENDOR experiments was constructed as a cylinder (0.5 mm wall thickness) of 11.0 mm inner diameter from iron free brass. The height of the cylindrical cavity on resonance (34 GHz) is 9.0 mm (determined with a Wilmad high precision 3 mm o.d. (2.0 mm i.d.) quartz sample tube inserted). This ensures a high conversion of incident microwave power to microwave field amplitude inside the cavity. The modular design of the resonator allows easy exchange of different resonator bodies (Fig. 1a, see below). For pulse EPR experiments it is important to obtain a resonance bandwidth of more than 20 MHz. Therefore the brass cylinder was not gold coated and the Iris for coupling

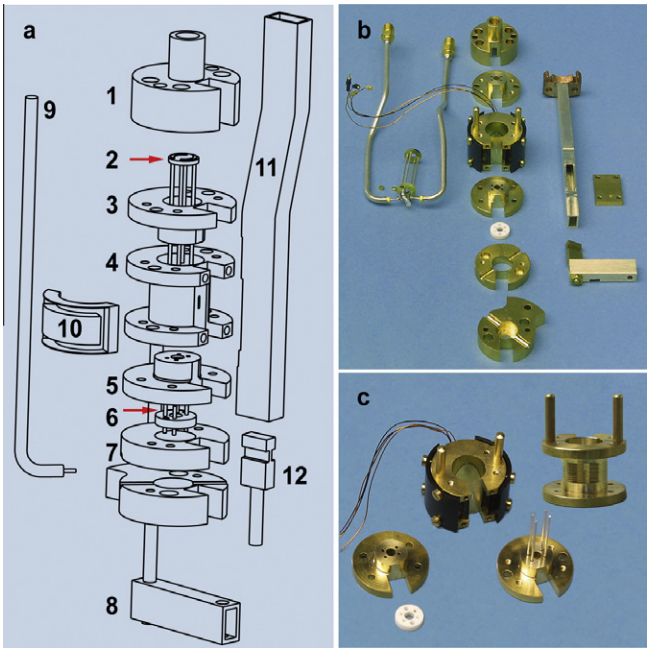

Fig. 1. (a) Exploded view of the Q-band TE_{011} ENDOR resonator probehead; (1) Upper cover; (2) ENDOR posts; (3) upper (movable) plunger; (4) resonator body with iris on the right (flattened) side; (5) lower (fixed) plunger; (6) RF contact plate; (7) coax clamps; (8) drive bar for sliding short; (9) RF coax line; (10) modulation coil body; (11) coupling wave guide; (12) sliding short. (b) Photo of the disassembled resonator showing the parts in panel (a). The input and output coax lines are connected to the ENDOR coil and the modulation coils are mounted to the resonator body. (c) Photo of the resonator body with modulation coil attached (using the black caps). The upper and lower plunger, detailing also the silver posts making up the RF coil as well as the MACOR contact plate (white). In addition a "naked" resonator body with slits (12 cuts of 0.3 mm, 0.5 mm apart giving a 3 mm wide 60% optical access) is shown.

the microwave from the waveguide into the cavity was slightly enlarged (2.5 × 0.5 mm slot, see Fig. 1, part ⟨4⟩) in order to lower the quality factor Q of the resonator. For continuous wave (CW) EPR/ENDOR measurements the Q of the resonator should be as high as possible (loaded quality factor, Q_L = 2600) and a large field modulation amplitude should be achieved (1 mT). For this application a second resonator body was built from high density graphite. The cylinder (Fig. 1, part ⟨4⟩) was polished and gold coated from the inside using electro plating. The graphite body allows a 100 kHz skin depth of 5.8 mm (at room temperature) while the wall thickness was not more than 1.5 mm. Therefore, the modulation field produced by the external coils was virtually undamped. Later in the development process a third "multi-purpose" (CW and pulse EPR) body was constructed from iron-free brass with three deep slots (0.2 mm) in order to suppress the Eddy-currents generated by the modulation coils. Also in this resonator (Q_L = 1300–2600), the modulation field was virtually undamped. This body, however, does not contain an optical window.

Both plungers (Fig. 1, parts ⟨3⟩ and ⟨5⟩) were made from iron-free brass. In the plunger heads a 3.2 mm hole for the sample tubes was machined as well as 0.8 mm holes for the four silver ENDOR posts (Fig. 1, part ⟨2⟩) which were electrically insulated from the plunger by 0.1 mm PEEK (polyether ether ketone) sealing tubes. The upper plunger was movable to allow for frequency tuning. The lower plunger was fixed to the resonator and contained the contact plate for connecting the ENDOR posts to the RF line. The RF power was delivered to the ENDOR coil through 2.8 mm semi-rigid coax lines which were firmly clamped to the resonator assembly and soldered to the contact plate. The resonator body itself was attached to the Ka-band (WR28) coupling waveguide (Fig. 1, part ⟨11⟩). The iris was machined into the flattened side of the cavity

[1] The same (sealed) quartz 3 mm o.d. tube can also be used in our EPR setup at 244 GHz [21] in a non-resonant sample holder.

body thereby reducing the thickness of the cavity wall to less than 0.1 mm at the side of the iris. A sliding short (Fig. 1, part ⟨12⟩) was used at the end of the waveguide to facilitate variable matching of the microwave coupling to the resonator for fixed iris dimensions. The movable plunger as well as the sliding short were operated through lever mechanisms at the top flange of the Oxford instruments CF935 cryostat insert which allows tuning of the resonance frequency and the microwave coupling between room temperature and 4 K. In Fig. 1 the overall assembly of the resonator is presented.

2.1. The tuning and coupling mechanisms

The movable top plunger ⟨3⟩ is attached to the upper mounting body ⟨1⟩ which in turn is connected to the inner support tube made from G10/FR4 (glass fiber reinforced epoxy, not shown) and ensures thermal insulation when the resonator is cooled to 4 K. The plunger is sliding along two rods fixed in the cavity body ⟨4⟩. The guidance of the plunger was sufficiently accurate to prevent touching the inner cylinder wall, which would create unwanted resonance modes. The G10/FR4 sample rod slides inside the inner support tube and passes the top flange of the insert, which connects to the cryostat through several O-rings (not shown). The inner support tube and the attached top plunger are driven by a stainless steel lever at the top of the insert. The coupling waveguide ⟨11⟩ was constructed from a piece of solid silver WR28 guide shaped into an offset-bend (ca. 5 mm offset). The short sidewall of the guide was machined out to accommodate the resonator cylinder side wall containing the iris. The sliding short was made from a rectangular iron-free brass plug ⟨12⟩ containing a choke to prevent microwave leakage. The short is driven by a bar ⟨8⟩ guided through a hole in the lower mounting body ⟨7⟩ containing a cross bar made from waveguide material on which the short plug was attached. The coupling drive bar was operated through a similar lever from the top of the resonator support insert as used for the tuning mechanism.

2.2. RF coil

The RF coil ⟨2⟩ was made from four 0.8 mm solid silver posts supported at the upper end by an epoxy mounting plate with the proper electrical cross connections. The geometry of the posts follows a pseudo Helmholtz geometry (see Table 1). The posts are passing through the four holes in the top and bottom plunger and are guided through inserts made from PEEK pressed inside the hollow plunger heads (not shown). This way electrical contact or sparking to the plungers under high power ENDOR operation is prevented. The lower ends of the posts are not soldered but inserted into four contact bushes pressed into a PCB plate which is attached to the PEEK insert in the bottom plunger. While the top plunger can move freely along the ENDOR posts the bottom plunger is fixed and provides the anchoring point of the ENDOR coil. The input and output coax lines are made from 3.6 mm semi-rigid cable RG-402/4 (silver plated copper inner and outer conductor). The lower parts of the coax lines are made from flexible semi-rigid cable (Sucoform 141) to allow for the 10 mm (radius) bends. The RF coax lines are clamped between the intermediate and lower mounting plate ⟨7⟩ and soldered to the contact plate. In the standard configuration of the RF coil the output coax line is terminated with a 50 Ω load. For low frequencies (<30 MHz) a configuration where the output coax line is shorted (at the RF coil) gives higher ENDOR efficiency, while for higher frequencies the terminated configuration provides a better impedance matching. In order to achieve good thermal insulation, from a position about 5 cm above the resonator up to the top of the resonator support insert, a different RF coax line is used (silver plated beryllium inner conductor, stainless steel outer conductor). For the same distance a thermal insulating microwave waveguide from stainless steel was used, whose inner walls were coated with gold (a few micrometers thick) for high microwave conductivity. Thereby a very good overall thermal insulation of the whole setup was obtained allowing operation of the resonator at 4 K inside the cryostat for many hours without having condensed water on the top of the resonator support outside the cryostat.

Table 1
Technical parameters for the Q-band TE_{011} CW/pulse ENDOR resonator.

MW frequency	32–36 GHz	RF frequency	1–400 MHz
Cavity diameter	11 mm	ENDOR geometry	2.7 × 4.6 mm [a]
Q_L (empty 3 mm tube)	1300–2600	Coil inductivity	0.5 μH
Modulation coil	30 turns	Sample tube diameter	3 mm
B_{mod} (100 kHz)	1 mT	Sample height	9 mm
(π/2) pulse (3 W)	20 ns	π-pulse RF, ^{1}H, 300 W	~20 μs

[a] The distance between two ENDOR posts forming one single loop coil is 4.6 mm. The distance between the two single loops is 2.7 mm (for an ideal Helmholtz case, these distances would have a ratio of 2:1). i.e. the holes in the plunger for the ENDOR posts are at the edges of a rectangle, with 4.6 mm (long side) and 2.7 mm (short side). The sample bore is in the center of this rectangle.

2.3. Field modulation

The field modulation coils were positioned outside the resonator. The coils were wound inside two PVC bodies ⟨10⟩ adapted to the shape of the resonator cylinder. In the original design the cavity body was constructed from iron-free brass. In this case the penetration of the modulation field is significantly reduced by the skin depth of brass. For pulse EPR/ENDOR experiments the field modulation capability is however not essential and the modulation coils were only occasionally used to find the EPR signal prior to subsequent advanced pulse measurements. For CW EPR/ENDOR experiments the field modulation performance is important, and therefore we constructed a special version of the resonator made from high density graphite [SGL Carbon Group, Grade R8340] which was electro-plated with 10–15 μm of gold. The advantage of graphite as cavity material is that the conductivity (specific resistance 1200 μΩ cm) is sufficient to enable electro-plating but is low enough to prevent damping of the modulation field. The skin depth of a 100 kHz signal is about 5.5 mm while the cavity wall is 1.5 mm thick. This compares to a skin depth of 0.4 mm at 100 kHz for brass. In addition, high density graphite is easy to machine and even allows the application of screw holes into the body. An additional cavity body (without optical access) from iron-free brass was built for improved field modulation by applying deep cuts 75% through the cylinder to suppress Eddy-currents. This strategy also allowed for large field modulation amplitudes (1.7 mT at 100 kHz).

2.4. Light access

In order to allow for optical excitation of the sample in combination with EPR/ENDOR, 12 slits of 0.3 mm width (3 mm long) at 0.2 mm distance were machined into the resonator body as shown in Fig. 1c. This provided optical transmission of ~60% while the Q value of the resonator was not reduced. This procedure was applied for both the brass and the graphite body. Due to the robust construction of the resonator, light energy in excess of 200 mJ at 355 nm (20 ns, 10 Hz, 3 mm spot) could be applied.

3. Performance of the resonator

The resonator was designed to be used with the Bruker Elexsys E680 Q-band FT EPR spectrometer, which in the basic version provides 3 W microwave power. Under these conditions, the shortest π/2 pulse duration in the overcoupled resonator (Q_L = 1600)

was determined as approximately 20 ns using a coal sample at room temperature. This is obtained from the observed spin nutations at the respective mw power as shown in Fig. 2.

The bandwidth of the resonator was determined experimentally by observing the reflection of a test pulse from the resonator as a function of the position of the short using the method described in [22]. The voltage decay trace of the reflected pulse (see Fig. S1) was fitted with an exponential providing the ringing time (T_R). From this the bandwidth of the resonator can be calculated as BW = $1/(\pi T_R)$. From the reflected voltage during the test pulse (positive of negative) the coupling parameter β of the resonator was determined. $\beta > 1$ (positive reflection) indicates under-coupling while $\beta > 1$ (positive reflection) indicates over-coupling. The variation of the bandwidth and coupling parameter with the position of the short is depicted in Fig. 3. Obviously, by increasing the size of the coupling iris, the bandwidth of the resonator can be increased further, but this will be at the expense of power conversion and sensitivity. It is clear that the ringing time of the resonator will affect the dead-time of the spectrometer. The actual dead-time of the pulse experiment will also depend on the noise floor of the detection system and the incident power on the resonator. In practice, for the Bruker Elexsys E580 system we observed a shortest time τ in a two-pulse echo experiment of around 300 ns.

The field modulation depth inside the resonator was determined from the "overmodulation" distortion effect on the lineshape of 2,2-diphenyl-1-picryl-hydrazyl (DPPH). Even with the standard configuration (1.5 mm solid brass resonator body) a field modulation of 0.45 mT at 10 kHz could be achieved (see Fig. S2a). In a similar experiment on a brass resonator with 3 slots 0.2 mm wide (no optical window) as well as the graphite resonator a larger modulation amplitude was reached at 100 kHz (e.g. 1.7 mT, see Fig. S2b).

The microwave field distribution inside the resonator was probed using a Li:LiF crystallite [23] (resonating at $g = 2$) serving as point sample. For every position of the sample along the long axis of the resonator the nutation pattern of the free induction decay as a function of the length of a 3 W resonant microwave pulse was detected. In Fig. S3 the microwave nutation frequency (obtained by FFT) is plotted as a function of the sample position. The maximum field (21 MHz, 0.75 mT) corresponds to a $\pi/2$ pulse of 12 ns. Obviously, this time is significantly shorter than the $\pi/2$ pulse-length determined on the coal sample (18 ns) in Fig. 2. This difference can be explained by the inhomogeneity of the B_1 field along the z-axis which is inherent to the TE_{011} resonator. Fig. S3 also shows the profile of the RF field at 51.5 MHz, 250 W inside the resonator. This was obtained using a calibrated pickup coil (1 mm diameter) which was moved along the resonator axis while the RF coil was excited at 51.5 MHz. The maximum field in the rotating frame was 0.5 mT (21 kHz for ^{1}H NMR) which corresponds to a RF $\pi/2$-pulse of 24 μs in agreement with the nuclear nutation experiment (see below) shown in Fig. 4.

The ENDOR performance of the resonator was tested using a sample of 0.1% bisdiphenylene-β-phenyl allyl (BDPA) in polystyrene at room temperature. Fig. 4 shows the RF nutation traces recorded using a Davies ENDOR experiment [24] with variable length of the RF pulse which was tuned to the high frequency ^{1}H ENDOR signal at 55 MHz (Fig. 4, inset). In this experiment the ENDOR coil was terminated in 50 Ω. Depending on the used RF amplifier, the π_{RF} pulse length varies between 23 μs (300 W) and 7 μs (2500 W). Table 1 summarizes the key specifications of our Q-band TE_{011} EPR/ENDOR resonator.

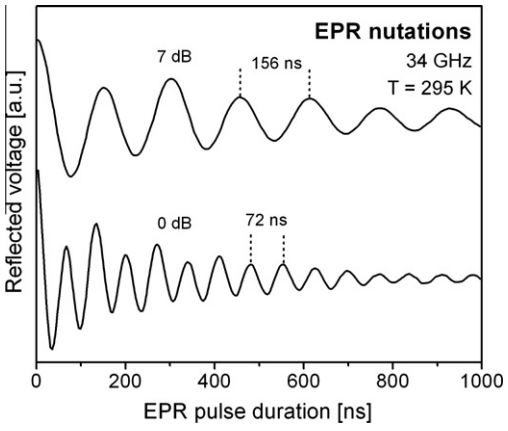

Fig. 2. EPR nutation experiments at room temperature performed on a coal sample. Experimental conditions: Field: 1211.3 mT, MW frequency: 33.9750 GHz, MW power: 0 dB = 3 W. Pulse sequence (7 dB): (variable pulse)–10 μs–$\pi/2$ (48 ns)–τ (600 ns)–π (88 ns)–τ (600 ns)–echo; (0 dB): same sequence but $\pi/2 = 24$ ns, $\pi = 48$ ns.

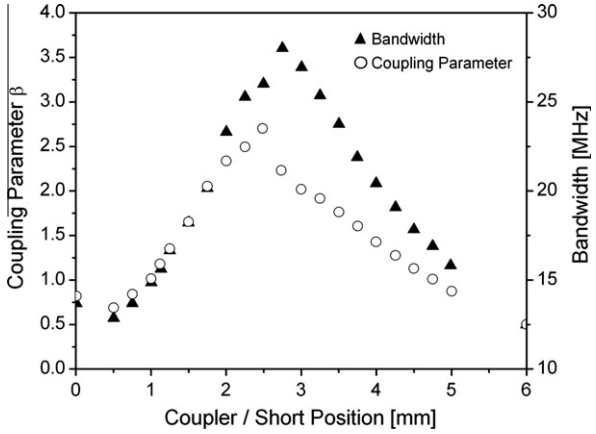

Fig. 3. Bandwidth and coupling parameter of the TE_{011} Q-band resonator as a function of the position of the sliding short with respect to the center of the iris hole. The coupling parameter β is equal to the voltage standing wave ratio (VSWR) in case of over-coupling and 1/VSWR in case of under-coupling. For critical coupling β = VSWR = 1.

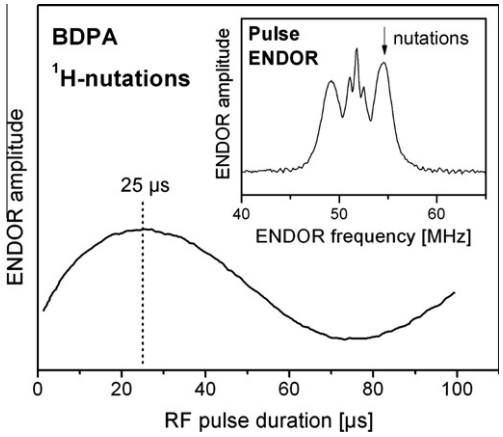

Fig. 4. ENDOR nutation experiment, using the full power (300 W) from an ENI A300 amplifier on BisDiphenylene-β-Phenyl Allyl (BDPA) at room temperature and using the Davies ENDOR sequence: $(\pi)_{mw}$–T_{rf}–$(\pi)/2_{mw}$–τ–$(\pi)_{mw}$–τ–echo; $(\pi)_{mw}$ = 160 ns, T_{rf} = 103 μs, τ = 1 μs. Other experimental conditions: T = 100 K, Field: 1214.0 mT, MW frequency: 34.0639 GHz, RF frequency : 54.5 MHz, Inset: Davies ENDOR experiment on BDPA at room temperature using an ENI A300 RF amplifier and an RF pulse length of 20 μs. The ENDOR coil was terminated in 50 Ω. $(\pi)_{mw}$ = 168 ns, T_{rf} = 20 μs, τ = 500 ns.

The spin concentration sensitivity that can be reached with our resonator as compared to that of the dielectric Bruker resonator (EN5107-D2) was estimated using a sample of 0.1% BDPA in polystyrene powder (determined as approximately 0.75 mM in spins). A two pulse echo sequence was applied at room temperature with $t_{\pi/2}$ = 40 ns and τ = 300 ns. The repetition rate was 1 ms. Both resonators were tuned to the same frequency (33.4 GHz) and coupled critically (Q = 2000 for TE_{011} vs Q = 1100 for the dielectric resonator). The sample was loaded in a 1.6 mm (o.d.) × 1.0 mm (i.d.) quartz tube for the dielectric resonator and a 3.0 mm (o.d.) × 2.0 mm (i.d.) tube for the TE_{011} resonator. Assuming the same effective height the sample volume is approximately four times larger in our resonator. In the Bruker resonator the signal to noise ratio of the single shot integrated echo intensity was 60. Taking into account the linewidth of 0.8 mT one can estimate a spin concentration sensitivity of approximately 15 μM/mT (single shot echo) at room temperature. In our TE_{011} resonator the single shot S/N was 210, i.e. 3.5 times higher. This would result in a 10 times shorter measuring time. Taking into account only the difference in volume and quality factor, a S/N improvement of a factor 7.3 would be expected. The "missing" factor of 2.1 is due to the better filling factor of the Bruker resonator. Hence, in practice, the large volume of the TE_{011} resonator overcompensates its poorer filling factor.

4. Applications

The resonator has been constructed and used continuously in our laboratory over the last decade for different Q-band EPR and ENDOR experiments both in CW and pulse mode. This is illustrated below by several examples on radicals, triplet states and transition metal centers in biological system.

4.1. Radicals

A large number of different radicals and radical ions, in particular in biological samples have been studied using the Q-band resonator. This provided a better g tensor resolution and increased orientation selection in related ENDOR experiments. Interesting applications are found among quinone radical ions [25–31], for which for example the hydrogen bond geometry was studied in deuterated solvents using ^{2}H CW and pulse ENDOR in frozen solutions at 80 K [25,26,29]. The linewidths in these experiments (~80 kHz) was sufficiently small to allow resolution of both the electron-nuclear hyperfine and the nuclear quadrupole tensors of the ^{2}H nuclei. Together with DFT calculations [26,32] these data provided detailed insight into strength and geometry of the H-bonds.

4.2. Photoexcited triplet states

The detection of light-induced radical pairs and triplet states by EPR and ENDOR represents a particular challenge due to the frequently encountered short life times. Several examples have been studied with the resonator described [30,33–36]. Fig. 5 shows the Q-band field-swept echo-detected EPR and ^{1}H Davies ENDOR spectra of a photoexcited triplet state. Light excitation was done *in situ* using a pulsed YAG laser in combination with an optical parametric oscillator (OPO), delivering 8 ns pulses of 5 mJ at 630 nm. The sample was illuminated in the resonator placed inside the EPR cryostat through the resonator slits/windows. The system chosen here is the triplet state of a carotenoid, peridinin in the Peridinin-Chlorophyll-Protein (PCP) antenna of the dinoflagellate *Amphidium carterae* [33]. The spin-polarized EPR spectrum results from fast triplet–triplet transfer from excited chlorophyll to peridinin, which *in vivo*

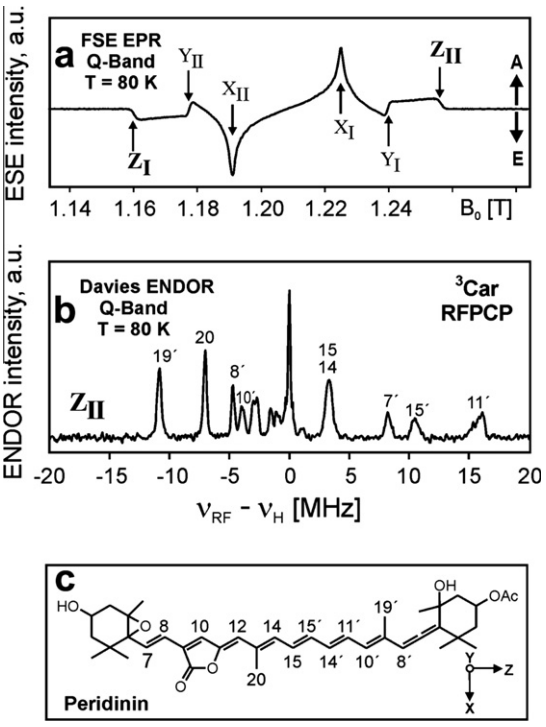

Fig. 5. (a) Time resolved Q-band field-swept echo-detected EPR and (b) ^{1}H Davies ENDOR spectra of the spinpolarized triplet state of the carotenoid peridinin (c) in the Peridinin-Chlorophyll Protein (PCP) antenna of *Amphidinium carterae* generated with a short laser flash (~10 ns duration); the delay after flash was 500 ns, the rf pulse length 6 μs (at 1500 W) and the mw pulse lengths 200, 40, 80 ns; for further details see [33].

serves to quench harmful chlorophyll triplet states that might occur in the process of photosynthetic light harvesting. The decay of the carotenoid triplet takes places in a few microseconds. The short triplet life time represents a challenge for ENDOR detection of the hyperfine couplings and the spin density distribution. In Fig. 5 it is shown that such experiments are feasible. Using the designed rf coils in combination with a high power rf amplifier (4 kW pulsed, 2.5 kW CW, Amplifier Research model 2500L) allows rf π-pulses of 6 μs length, sufficient for the detection of ^{1}H ENDOR of many short lived triplet states as those of carotenoids. Furthermore, stochastic ENDOR detection was used to diminish RF-dependent temperature artifacts in the spectrum [37]; the changing background signals after triplet state relaxation were subtracted. Fig. 5b shows the resulting ^{1}H Davies ENDOR spectrum at a single-crystal like position (Z_{II}) in the EPR (Fig. 5a), determined by the dominant zero field splitting of the triplet state. Thirteen hyperfine coupling constants – including signs – could be obtained by similar orientation dependent ENDOR experiments. The ^{1}H hfcs were assigned to molecular positions via a comparison with DFT calculations. This led to the first determination of the complete spin density distribution of a carotenoid triplet state; for details see [33].

4.3. Metalloproteins

The developed Q-band resonator was also successfully employed in the study of several paramagnetic metalloproteins, see e.g. [18,20,38–41]. Fig. 6 shows a field-swept echo-detected EPR spectrum of the oxygen evolving complex (S_2 state) in photosystem II of oxygenic photosynthesis (membrane fragments, spinach). The detected so-called "multiline signal" stems from a tetranuclear manganese/calcium cluster (Mn_4O_5Ca) found in oxygenic photosynthesis, the locus of light-induced water oxidation in Nature. Electron spin coupling in the cluster leads to a ground state with

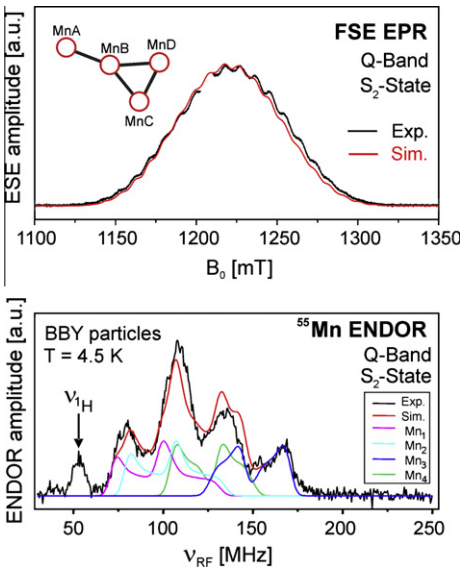

Fig. 6. Q-band field-swept echo-detected EPR (top) and ^{55}Mn Davies ENDOR (bottom) performed on the S_2 state of the water oxidizing complex of photosystem (PS) II (BBY particles, spinach) at $T = 4.5$ K. The ENDOR spectrum is simulated using four ^{55}Mn hyperfine couplings Mn_1 to Mn_4 (color coded). The simulation of the EPR multiline signal (top) was obtained by using all four hfcs (see text and [20]). Experimental conditions: Temperature 4.5 K, microwave frequency = 33.85 GHz, magnetic field = 1260 mT. RF pulse = 5 μs using a 100 W RF amplifier. Figure reprinted with permission form J. Am. Chem. Soc. 129 (2007) 13421–13435, copyright 2007 Americal Chemical Society.

an effective spin S = ½ leading to over 20 EPR lines due to coupling with the ^{55}Mn (I = 5/2) nuclei.

The lower panel shows the ^{55}Mn ENDOR spectrum (Davies ENDOR sequence) at Q-band that could be simulated with four ^{55}Mn hyperfine tensors, showing that all four manganese nuclei are coupled and contribute almost equally to the EPR and ENDOR spectra. The analysis and further work [42–44] led to an assignment of the spin and oxidation states and a spin coupling model of the manganese cluster. The ^{55}Mn ENDOR spectra were recorded using the stochastic acquisition mode in order to avoid heat induced baseline fluctuations [37].

The Q-band EPR/ENDOR resonator was also used in the study of the emzyme hydrogenase and related models [18,19,38,39,45–49]. For example, the H-cluster of [FeFe] hydrogenase was enriched in ^{57}Fe and analyzed using Davies (triple) ENDOR and ^{57}Fe HYSCORE. The simulations allowed the determination of all six ^{57}Fe hyperfine tensors (and their relative signs). This led to a solid model of the electronic structure of this important type of hydrogenase [18,38,45].

Although the bandwidth of the current resonator is limited to 30 MHz, this proved sufficient for successful ELDOR-detected NMR studies, for example to detect the ^{61}Ni hyperfine coupling parameters in [NiFe] hydrogenase [50]. It was demonstrated that especially for large hyperfine interactions this method has superior sensitivity over ENDOR. The analysis of the spectra by computer simulations yielded both the principal components of the hfc tensor and its orientation (i.e. Euler angles) with respect to the principal axes of the *g*-tensor, whose orientation is known from single crystal EPR experiments [51].

5. Conclusions and outlook

The developed general purpose frequency tunable Q-band TE_{011} ENDOR resonator described in this paper combines a large sample volume with high sensitivity and efficient pulse and CW ENDOR performance. The four fold increase in sample volume as compared to the commercial Bruker dielectric resonator, more than compensates the less favorable power conversion factor of this resonator. Furthermore, the availability of the large sample volume (3.0 mm o.d.) facilitates the study of "precious" biological samples simultaneously at X- and Q-band frequencies with satisfactory sensitivity.[2] The robust design of the ENDOR coil allows high power RF pulses (2500 Watts) and CW RF irradiation (500 W). The sample can be irradiated inside the resonator during EPR/ENDOR measurements at low temperature with a laser pulse energy up to 200 mJ (20 ns, 10 Hz) at 355 nm without problems. The dimensions of the probehead, i.e. resonator with glass fiber reinforced epoxy support, microwave waveguide and RF connections are fully compatible with an Oxford instruments CF935 helium flow cryostat (4–300 K) and can for example be directly connected to a Bruker Elexsys series Q-band FT EPR spectrometer. The described examples in which the probehead was employed in the study of organic radicals, photoexited triplet states and multinuclear transition metal complexes using steady-state and time resolved EPR, pulse EPR, ESEEM and HYSCORE, ENDOR and ELDOR-detected NMR spectroscopy are only a brief selection of the successful studies conducted with this resonator. It is clear that due to the passive coupling scheme using a sliding short, the bandwidth range of the current resonator is rather limited making it less suitable for PELDOR and high power pulse experiments. To alleviate this limitation, we are currently exploring the introduction of a physical coupling element (e.g. a conducting sphere) while maintaining the simplicity and robustness of the present design. A first account of this work will be published shortly (Savitsky, Grishin, Rakhmatullin, Reijerse, and Lubitz, 2012, in preparation).

Appendix A. Supplementary material

Supplementary data associated with this article can be found, in the online version, at doi:10.1016/j.jmr.2011.11.011.

References

[1] C.P. Poole, Electron Spin Resonance: A comprehensive treatise on experimental techniques, John Wiley, New York, 1983; second ed. Dover, New York, 1996.
[2] K.P. Dinse, K. Möbius, R. Biehl, Influence of coherence effects on line shapes in endor spectrum of perinaphthenyl radical, Z. Naturforsch. A 28 (1973) 1069–1080.
[3] R. Biehl, W. Lubitz, K. Möbius, M. Plato, Observation of deuterium quadrupole splittings of aromatic free radicals in liquid crystals by ENDOR and TRIPLE resonance, J. Chem. Phys. 66 (1977) 2074–2078.
[4] W. Lubitz, R.A. Isaacson, E.C. Abresch, G. Feher, ^{15}N electron nuclear double-resonance of the primary donor cation radical P_{865}^{+} in reaction centers of *Rhodopseudomonas sphaeroides*: additional evidence for the dimer model, Proc. Nat. Acad. Sci. USA 81 (1984) 7792–7796.
[5] W. Möhl, E. De Boer, ENDOR-probehead for weakly coupled nuclei with low magnetic-moments, J. Phys. E: Sci. Instrum. 18 (1985) 479–481.
[6] E.J. Reijerse, A.A.K. Klaassen, A variable temperature ESE-ENDOR resonator for single-crystal studies, Rev. Sci. Instrum. 57 (1986) 2768–2770.
[7] J. Hüttermann, R. Kappl, ENDOR – probing the coordination environment in metalloproteins, Met. Ions Biol. Syst. 22 (1987) 1–80.
[8] W. Zweygart, R. Thanner, W. Lubitz, An improved TM_{110} ENDOR cavity for the investigation of transition metal complexes, J. Magn. Res. Ser. A 109 (1994) 172–176.
[9] C.W.M. Kay, Y.A. Grishin, S. Weber, K. Möbius, An improved TM_{110} resonator for continuous-wave ENDOR studies at X-band, Appl. Magn. Res. 31 (2007) 599–609.
[10] C.E. Davoust, P.E. Doan, B.M. Hoffman, Q-band pulsed electron spin-echo spectrometer and its application to ENDOR and ESEEM, J. Magn. Res. Ser. A 119 (1996) 38–44.
[11] A. Sienkiewicz, B.G. Smith, A. Veselov, C.P. Scholes, Tunable Q-band resonator for low temperature electron paramagnetic resonance/electron nuclear double resonance measurements, Rev. Sci. Instrum. 67 (1996) 2134–2138.
[12] I. Gromov, J. Forrer, A. Schweiger, Probehead operating at 35 GHz for continuous wave and pulse electron paramagnetic resonance applications, Rev. Sci. Instrum. 77 (2006) 064704.

[2] The same 3 mm sample can also be accommodated in a non-resonant probehead of our high frequency (244 GHz) EPR setup [21].

[13] J. Forrer, I. García-Rubio, R. Schuhmann, R. Tschaggelar, J. Harmer, Cryogenic Q-band (35 GHz) probehead featuring large excitation microwave fields for pulse and continuous wave electron paramagnetic resonance spectroscopy: performance and applications, J. Magn. Reson. 190 (2008) 280–291.
[14] R. Tschaggelar, B. Kasumaj, M.G. Santangelo, J. Forrer, P. Leger, H. Dube, F. Diederich, J. Harmer, R. Schuhmann, I. García-Rubio, G. Jeschke, Cryogenic 35 GHz pulse ENDOR probehead accommodating large sample sizes: performance and applications, J. Magn. Reson. 200 (2009) 81–87.
[15] I. Tkach, A. Baldansuren, E. Kalabukhova, S. Lukin, A. Sitnikov, A. Tsvir, M. Ischenko, Y. Rosentzweig, E. Roduner, A homebuilt ESE spectrometer on the basis of a high-power Q-band microwave bridge, Appl. Magn. Res. 35 (2008) 95–112.
[16] W. Lubitz, F. Lendzian, R. Bittl, Radicals, Radical Pairs and triplet states in photosynthesis, Acc. Chem. Res. 35 (2002) 313–320.
[17] L.V. Kulik, B. Epel, J. Messinger, W. Lubitz, Pulse EPR, ^{55}Mn-ENDOR and ELDOR-detected NMR of the S_2-state of the oxygen evolving complex in photosystem II, Photosynth. Res. 84 (2005) 347–353.
[18] A. Silakov, E.J. Reijerse, S.P.J. Albracht, E.C. Hatchikian, W. Lubitz, The electronic structure of the H-cluster in the [FeFe]-hydrogenase from *Desulfovibrio desulfuricans*: a Q-band ^{57}Fe ENDOR and HYSCORE study, J. Am. Chem. Soc. 129 (2007) 11447–11458.
[19] W. Lubitz, E. Reijerse, M. van Gastel, [NiFe] and [FeFe] hydrogenases studied by advanced magnetic resonance techniques, Chem. Rev. 107 (2007) 4331–4365.
[20] L.V. Kulik, B. Epel, W. Lubitz, J. Messinger, Electronic structure of the Mn_4O_xCa cluster in the S_0 and S_2 states of the oxygen-evolving complex of photosystem II based on pulse ^{55}Mn ENDOR and EPR spectroscopy, J. Am. Chem. Soc. 129 (2007) 13421–13435.
[21] E. Reijerse, P.P. Schmidt, G. Klihm, W. Lubitz, A CW and pulse EPR spectrometer operating at 122 and 244 GHz using a quasi-optical bridge and a cryogen-free 12 T superconducting magnet, Appl. Magn. Res. 31 (2007) 611–626.
[22] N.I. Avdievich, G.J. Gerfen, Multifrequency probe for pulsed EPR and ENDOR spectroscopy, J. Magn. Reson. 153 (2001) 178–185.
[23] A. Stesmans, G. Vangorp, Novel method for accurate *g* measurements in electron-spin resonance, Rev. Sci. Instrum. 60 (1989) 2949–2952.
[24] E.R. Davies, A new pulse ENDOR technique, Phys. Lett. A 47 (1974) 1–2.
[25] M. Flores, R.A. Isaacson, R. Calvo, G. Feher, W. Lubitz, Probing hydrogen bonding to quinone anion radicals by ^{1}H and ^{2}H ENDOR spectroscopy at 35 GHz, Chem. Phys. 294 (2003) 401–413.
[26] S. Sinnecker, E. Reijerse, F. Neese, W. Lubitz, Hydrogen bond geometries from electron paramagnetic resonance and electron-nuclear double resonance parameters: density functional study of quinone radical anion–solvent interactions, J. Am. Chem. Soc. 126 (2004) 3280–3290.
[27] M. Flores, R. Isaacson, E. Abresch, R. Calvo, W. Lubitz, G. Feher, Protein-cofactor interactions in bacterial reaction centers from *Rhodobacter sphaeroides* R-26: I. Identification of the ENDOR lines associated with the hydrogen bonds to the primary quinone $Q_A^{\bullet-}$, Biophys. J. 90 (2006) 3356–3362.
[28] B. Epel, J. Niklas, S. Sinnecker, H. Zimmermann, W. Lubitz, Phylloquinone and related radical anions studied by pulse electron nuclear double resonance spectroscopy at 34 GHz and density functional theory, J. Phys. Chem. B 110 (2006) 11549–11560.
[29] M. Flores, R. Isaacson, E. Abresch, R. Calvo, W. Lubitz, G. Feher, Protein-cofactor interactions in bacterial reaction centers from *Rhodobacter sphaeroides* R-26: II. Geometry of the hydrogen bonds to the primary quinone $Q_A^{\bullet-}$ by ^{1}H and ^{2}H ENDOR spectroscopy, Biophys. J. 92 (2007) 671–682.
[30] J. Niklas, B. Epel, M.L. Antonkine, S. Sinnecker, M.E. Pandelia, W. Lubitz, Electronic structure of the quinone radical anion $A_1^{\bullet-}$ of photosystem I investigated by advanced pulse EPR and ENDOR techniques, J. Phys. Chem. B 113 (2009) 10367–10379.
[31] M. Flores, A. Savitsky, M.L. Paddock, E.C. Abresch, A.A. Dubinskii, M.Y. Okamura, W. Lubitz, K. Möbius, Electron–nuclear and electron–electron double resonance spectroscopies show that the primary quinone acceptor Q_A in reaction centers from photosynthetic bacteria *Rhodobacter sphaeroides* remains in the same orientation upon light-induced reduction, J. Phys. Chem. B 114 (2010) 16894–16901.
[32] S. Sinnecker, M. Flores, W. Lubitz, Protein–cofactor interactions in bacterial reaction centers from *Rhodobacter sphaeroides* R-26: effect of hydrogen bonding on the electronic and geometric structure of the primary quinone. A density functional theory study, Phys. Chem. Chem. Phys. 8 (2006) 5659–5670.
[33] J. Niklas, T. Schulte, S. Prakash, M. van Gastel, E. Hofmann, W. Lubitz, Spin-density distribution of the carotenoid triplet state in the peridinin-chlorophyll-protein Antenna. A Q-band pulse electron-nuclear double resonance and density functional theory study, J. Am. Chem. Soc. 129 (2007) 15442–15443.
[34] A. Marchanka, M. Paddock, W. Lubitz, M. van Gastel, Low-temperature pulsed EPR study at 34 GHz of the triplet states of the primary electron donor P_{865} and the carotenoid in native and mutant bacterial reaction centers of *Rhodobacter sphaeroides*, Biochemistry 46 (2007) 14782–14794.
[35] A. Marchanka, W. Lubitz, M. van Gastel, Spin density distribution of the excited triplet state of bacteriochlorophylls. Pulsed ENDOR and DFT studies, J. Phys. Chem. B 113 (2009) 6917–6927.
[36] B. Epel, J. Niklas, M.L. Antonkine, W. Lubitz, Absolute signs of hyperfine coupling constants as determined by pulse ENDOR of polarized radical pairs, Appl. Magn. Res. 30 (2006) 311–327.
[37] B. Epel, D. Arieli, D. Baute, D. Goldfarb, Improving W-band pulsed ENDOR sensitivity-random acquisition and pulsed special TRIPLE, J. Magn. Reson. 164 (2003) 78–83.
[38] A. Silakov, B. Wenk, E. Reijerse, W. Lubitz, ^{14}N HYSCORE investigation of the H-cluster of [FeFe] hydrogenase: evidence for a nitrogen in the dithiol bridge, Phys. Chem. Chem. Phys. 11 (2009) 6592–6599.
[39] M. Saggu, C. Teutloff, M. Ludwig, M. Brecht, M.E. Pandelia, O. Lenz, B. Friedrich, W. Lubitz, P. Hildebrandt, F. Lendzian, R. Bittl, Comparison of the membrane-bound [NiFe] hydrogenases from *R. eutropha* H16 and *D. vulgaris* Miyazaki F in the oxidized ready state by pulsed EPR, Phys. Chem. Chem. Phys. 12 (2010) 2139–2148.
[40] S.C. Drew, E.J. Reijerse, A. Quentmeier, D. Rother, C.G. Friedrich, W. Lubitz, Spectroscopic characterization of the molybdenum cofactor of the sulfane dehydrogenase SoxCD from *Paracoccus pantotrophus*, Inorg. Chem. 50 (2010) 409–411.
[41] N. Cox, H. Ogata, P. Stolle, E. Reijerse, G. Auling, W. Lubitz, A tyrosyl-dimanganese coupled spin system is the native metalloradical cofactor of the R2F subunit of the ribonucleotide reductase of *Corynebacterium ammoniagenes*, J. Am. Chem. Soc. 132 (2010) 11197–11213.
[42] N. Cox, L. Rapatskiy, J.H. Su, D.A. Pantazis, M. Sugiura, L.V. Kulik, P. Dorlet, A.W. Rutherford, F. Neese, A. Boussac, W. Lubitz, J. Messinger, Effect of Ca^{2+}/Sr^{2+} substitution on the electronic structure of the oxygen-evolving complex of photosystem II: a combined multifrequency EPR, ^{55}Mn-ENDOR, and DFT study of the S_2 state, J. Am. Chem. Soc. 133 (2011) 3635–3648.
[43] J.H. Su, N. Cox, W. Ames, D.A. Pantazis, L. Rapatskiy, T. Lohmiller, L.V. Kulik, P. Dorlet, A.W. Rutherford, F. Neese, A. Boussac, W. Lubitz, J. Messinger, The electronic structures of the S_2 states of the oxygen-evolving complexes of photosystem II in plants and cyanobacteria in the presence and absence of methanol, Biochim. Biophys. Acta 1807 (2011) 829–840.
[44] N. Cox, W. Ames, B. Epel, L.V. Kulik, L. Rapatskiy, F. Neese, J. Messinger, K. Wieghardt, W. Lubitz, Electronic structure of a weakly antiferromagnetically coupled $Mn^{II}Mn^{III}$ model relevant to manganese proteins: a combined EPR, ^{55}Mn-ENDOR, and DFT study, Inorg. Chem. 50 (2011) 8238–8251.
[45] A. Silakov, B. Wenk, E. Reijerse, S.P.J. Albracht, W. Lubitz, Spin distribution of the H-cluster in the H_{ox}–CO state of the [FeFe] hydrogenase from *Desulfovibrio desulfuricans*: HYSCORE and ENDOR study of ^{14}N and ^{13}C nuclear interactions, J. Biol. Inorg. Chem. 14 (2009) 301–313.
[46] M.E. Pandelia, H. Ogata, W. Lubitz, Intermediates in the catalytic cycle of [NiFe] hydrogenase: functional spectroscopy of the active site, ChemPhysChem 11 (2010) 1127–1140.
[47] A. Silakov, J.L. Shaw, E.J. Reijerse, W. Lubitz, Advanced electron paramagnetic resonance and density functional theory study of a {2Fe3S} cluster mimicking the active site of [FeFe] hydrogenase, J. Am. Chem. Soc. 132 (2010) 17578–17587.
[48] Ö.F. Erdem, L. Schwartz, M. Stein, A. Silakov, S. Kaur-Ghumaan, P. Huang, S. Ott, E.J. Reijerse, W. Lubitz, A model of the [FeFe] hydrogenase active site with a biologically relevant azadithiolate bridge: a spectroscopic and theoretical investigation, Angew. Chem. 50 (2011) 1439–1443.
[49] A. Silakov, E.J. Reijerse, W. Lubitz, Unraveling the electronic properties of the photoinduced states of the H-cluster in the [FeFe] hydrogenase from *D. desulfuricans*, Eur. J. Inorg. Chem. 2011 (2011) 1056–1066.
[50] M. Flores, A.G. Agrawal, M. van Gastel, W. Gärtner, W. Lubitz, Electron–electron double resonance-detected NMR to measure metal hyperfine interactions: ^{61}Ni in the Ni–B state of the [NiFe] hydrogenase of *Desulfovibrio vulgaris* miyazaki F, J. Am. Chem. Soc. 130 (2008) 2402–2403.
[51] S. Foerster, M. Stein, M. Brecht, H. Ogata, Y. Higuchi, W. Lubitz, Single crystal EPR studies of the reduced active site of [NiFe] hydrogenase from *Desulfiovibrio vulgaris* miyazaki F, J. Am. Chem. Soc. 125 (2003) 83–93.